Quark gluon plasma studies within a partonic transport approach

Florian Senzel[1], Moritz Greif[1], Jan Uphoff[1], Christian Wesp[1], Zhe Xu[2], Carsten Greiner[1]

[1]Goethe-Universität, Max-von-Laue-Str. 1, 60438 Frankfurt am Main, Germany
[2]Tsinghua University, Beijing 100084, China

Aiming for the simultaneous description of the hard and the soft regime of ultra-relativistic heavy-ion collisions, we present our recent findings within the partonic transport model BAMPS (Boltzmann Approach to Multi-Parton Scatterings). While using both elastic and radiative interactions provided by perturbative QCD, BAMPS allows the full 3+1D simulation of the quark-gluon plasma (QGP) at the microscopic level by solving the relativistic Boltzmann equation for quarks and gluons. BAMPS facilitates investigations of jet quenching, heavy flavor and elliptic flow within the partonic phase of heavy-ion collisions as well as studies of QGP medium properties in terms of e.g. transport coefficients like η/s and the electric conductivity.

1 Introduction

When heavy nuclei collide at ultra-relativistic energies, a system of hot and dense matter is created. Due to the enormous available energy densities within these collisions, quasi-free quarks and gluons represent the relevant degrees of freedom. Therefore the produced medium is commonly called the "quark-gluon plasma" (QGP). Experiments at both the Relativistic Heavy-Ion Collider (RHIC) at BNL and the Large Hadron Collider (LHC) at CERN show that the created medium exhibits interesting properties [1]: While high energy particles traversing the medium are quenched, the system shows at the same time a collective behavior similar to a nearly perfect liquid. Among the most prominent observables for quantifying these properties are the nuclear modification factor, R_{AA}, and the elliptic flow, v_2. While R_{AA} measures the suppression of inclusive particle yields compared to scaled p+p collisions, the elliptic flow v_2, defined in terms of the second Fourier coefficient of the azimuthal particle distribution, gives insight to the collectivity of the medium.

Although both phenomena are commonly attributed to the partonic phase of the heavy-ion collision, a simultaneous understanding of jet quenching and bulk phenomena on the microscopic level remains a challenge. In this paper we report on our progress in understanding the QGP within the partonic transport model *Boltzmann Approach to Multi-Parton Scatterings* (BAMPS). Based on cross sections calculated in perturbative quantum chromodynamics (pQCD), soft and hard particles are treated on the same footing in a common framework. While we take explicitly the running of the coupling into account, we study the energy loss of highly energetic [2, 3] and heavy flavor particles [4, 5] as well as the collective behavior in terms of the elliptic flow [3] and the electric conductivity of the underlying QGP medium [6].

2   The BAMPS framework

The partonic transport model *Boltzmann Approach to Multi-Parton Scatterings* (BAMPS) [7, 8] describes the full 3+1D evolution of both the QGP medium as well as high energy particles traversing it by numerically solving the relativistic Boltzmann equation,

$$p^\mu \partial_\mu f(\vec{x}, t) = \mathcal{C}_{22} + \mathcal{C}_{2\leftrightarrow 3} \,, \tag{1}$$

for on-shell partons, quarks and gluons, and perturbative quantum chromodynamics (pQCD) interactions. To this end, a stochastical modeling of the collision probabilities together with a test-particle ansatz is employed.

Within BAMPS, both elastic $2 \to 2$ scattering processes calculated in leading-order pQCD, like e.g. $g\,g \to g\,g$, and inelastic $2 \leftrightarrow 3$ interactions, like e.g. $g\,g \leftrightarrow g\,g\,g$, are considered. The inelastic cross sections are calculated within an *improved Gunion-Bertsch (GB) approximation* [9, 10],

$$\left|\overline{\mathcal{M}}_{X\to Y+g}\right|^2 = 48\pi\alpha_s(k_\perp^2)\,(1-\bar{x})^2\,\left|\overline{\mathcal{M}}_{X\to Y}\right|^2 \left[\frac{\mathbf{k}_\perp}{k_\perp^2} + \frac{\mathbf{q}_\perp - \mathbf{k}_\perp}{(\mathbf{q}_\perp - \mathbf{k}_\perp)^2 + m_D^2\,(\alpha_s(k_\perp^2))}\right]^2 \,, \tag{2}$$

which agrees well with the exact pQCD matrix element over a wide phase space region [10]. As a remark, $\left|\overline{\mathcal{M}}_{X\to Y}\right|$ denotes the matrix element of the respective elastic process, while $k_\perp$ and $q_\perp$ are the transverse momentum of the emitted and internal gluons, respectively.

The running of the QCD coupling $\alpha_s(k_\perp^2)$ is considered within BAMPS by setting the scale of the coupling to the momentum transfer of the considered channel and thereby evaluating it for each collision at the microscopic level.

For modeling the Landau-Pomeranchuk-Migdal (LPM) effect, which is an important quantum effect within a partonic QCD medium, an effective cutoff function $\theta\,(\lambda - X_{LPM}\,\tau_f)$ in the radiative matrix elements is used, where λ is the mean free path of the radiating particle, τ_f the gluon formation time and X_{LPM} a parameter that effectively controls the independence between consecutive gluon emissions. The value $X_{LPM} = 0.3$ is fixed by comparing to R_{AA} data of neutral pions at RHIC [3]. Any further divergences occurring in the integration of the pQCD matrix elements are cured by a screening Debye mass m_D^2, which is dynamically computed on the basis of the current quark and gluon distribution [7].

3   Jet quenching within heavy-ion collisions

While employing PYTHIA [11] initial conditions together with a Monte Carlo Glauber sampling as described in detail in Ref. [7, 12], Fig. 1 (left) shows the nuclear modification factor R_{AA} obtained by BAMPS for gluons, light quarks and charged hadrons at the LHC [3]. Due to their larger QCD color factor, gluons are stronger suppressed than light quarks over the whole p_t range. For comparison with data, we also show the R_{AA} for charged hadrons resulting from fragmentation via AKK fragmentation functions [13]. According to this fragmentation functions, hadrons at low p_t are dominated by fragmenting gluons, while at higher p_t the quark contribution increases. Together with the rising shape of the R_{AA} this effect leads to a hadronic R_{AA} that is close to the quark R_{AA}.

Another method for characterizing the energy loss of high p_t partons within the QGP is the reconstruction of jets within heavy-ion collisions. Both the ATLAS [14] and CMS experiments
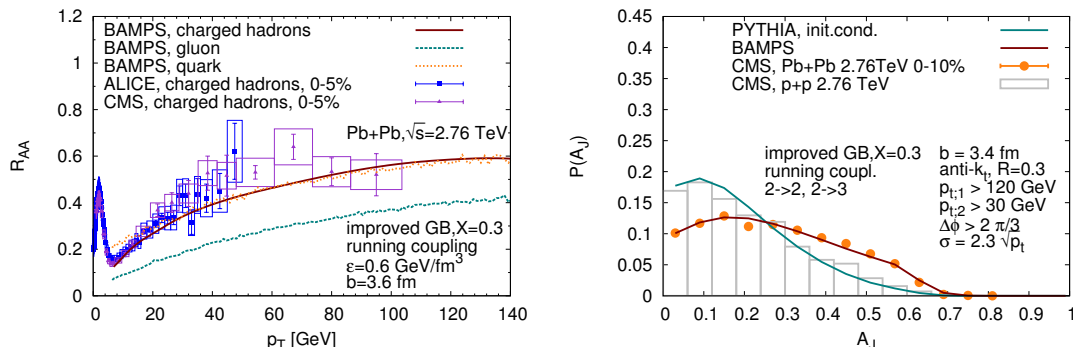
Figure 1: Left: Nuclear modification factor R_{AA} of gluons, light quarks, and charged hadrons at LHC (left) for a running coupling and LPM parameter $X = 0.3$ together with data of charged hadrons [16] as published in Ref. [3]. Right: A_J distribution calculated by BAMPS [2] with impact parameter $b_{\mathrm{mean}} = 3.4$ fm together with PYTHIA initial conditions in comparison with $\sqrt{s} = 2.76$ TeV p+p and $\sqrt{s} = 2.76$ ATeV 0-10% Pb+Pb data measured by CMS [15] as published in Ref. [2].

[15] reported the measurement of an enhanced number of events with an asymmetric pair of back-to-back reconstructed jets in comparison to p+p events, which is quantified in terms of the momentum imbalance $A_J (p_{t;1}, p_{t;2}) = \frac{p_{t;1} - p_{t;2}}{p_{t;1} + p_{t;2}}$, where $p_{t;1}$ ($p_{t;2}$) is the transverse momentum of the leading (subleading) jet—the reconstructed jet with the highest (second highest) transverse momentum per event. While employing all experimental trigger conditions, Fig. 1 (right) shows the momentum imbalance A_J calculated within BAMPS together with data. Consistent with the R_{AA} studies the momentum imbalance of reconstructed jets within BAMPS is in agreement with data. For more details about the studies of reconstructed jets within BAMPS we refer to Ref. [2].

4 Heavy flavor within heavy-ion collisions

Quantitative studies of heavy flavor within BAMPS [17, 18, 4] show that, although elastic processes with a running coupling and an improved screening procedure contribute significantly to the energy loss of heavy quarks, they alone cannot reproduce the data of the nuclear modification factor or the elliptic flow of any heavy flavor particle species. Therefore, before radiative heavy quark processes have been implemented in BAMPS, we mimicked their influence by effectively increasing the elastic cross section by a factor $K = 3.5$, which is tuned to the v_2 data of heavy flavor electrons at RHIC [4]. With this fixed parameter it is furthermore possible to describe the R_{AA} of heavy flavor electrons at RHIC as well as the experimentally measured R_{AA} and v_2 of all heavy flavor particles at LHC (see Fig. 2). However, the need of the phenomenological K factor is rather unsatisfying from the theory perspective. Therefore, the question arises whether radiative processes can account for the missing contribution parameterized by the K factor. To this end, we present in the left panel of Fig. 3 the nuclear modification factor at LHC calculated within BAMPS while treating both heavy and light partons on the same footing consisting of radiative processes based on the improved GB matrix element, a running
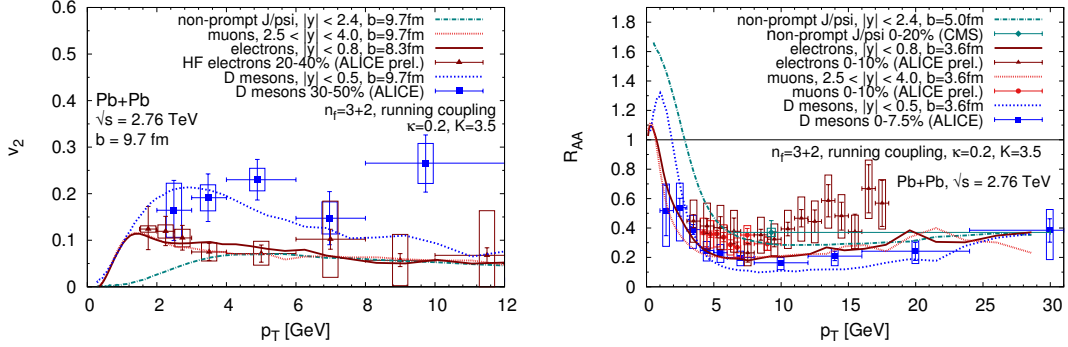
Figure 2: Elliptic flow v_2 (left) and nuclear modification factor R_{AA} (right) of various heavy flavor particles at LHC as published in Ref. [4] together with data [19, 20, 21, 22, 23, 24]. Only binary heavy flavor processes are considered and multiplied with $K = 3.5$.

coupling and an effective modeling of the LPM effect ($X_{LPM} = 0.3$) [5]. A good agreement between the BAMPS calculations and the nuclear modification factor of D mesons at LHC is found. As shown in Ref. [5] the energy loss of light and charm quarks is similar what explains why the nuclear modification factors of charged hadrons and D mesons in heavy-ion collisions have also the same values. Furthermore, mass effects in the fragmentation of gluons and light quarks to charged hadrons and charm quarks to D mesons lead to a similar suppression of charged hadrons and D mesons in BAMPS.

5   Properties of the underlying QGP medium

After presenting results on jet quenching and heavy flavor, we investigate the bulk evolution by employing the same setup as already described above together with the fixed LPM parameter $X_{LPM} = 0.3$ and a freeze-out energy density $\epsilon_c = 0.6 \, \text{GeV/fm}$ [26]. Since the microscopic hadronization processes within the soft regime are not fully understood yet, we show in Fig. 3 (right) our results for the integrated, partonic v_2 as a function of the number of participants N_{part} in comparison with LHC data.

Remarkably, by using the same microscopic pQCD interactions for both the hard and the soft momentum regime, BAMPS media build up a sizable amount of flow within the partonic phase. The reason for this lies in the isotropization of inelastic $2 \leftrightarrow 3$ processes as well as the running coupling, which affects the elliptic flow of particles with small p_T and the R_{AA} of particles with large p_T differently. The difference of the integrated, partonic v_2 of BAMPS and the measured, hadronic v_2 both at LHC is about $10-20\%$ and is supposed to be caused by the missing hadronic phase.

As advocated in dissipative hydrodynamic fits, an important quantity for the bulk medium in heavy-ion collisions is the shear viscosity to entropy density ratio η/s. In Fig. 4 (left) the temperature dependence of this value in a static medium allowing all $2 \to 2$ and $2 \leftrightarrow 3$ processes is shown. The shear viscosity is calculated via the Green-Kubo relation, which links the autocorrelation function of the medium energy-momentum tensor of the medium to the transport coefficient η [27]. The ratio η/s decreases with decreasing temperature and reaches
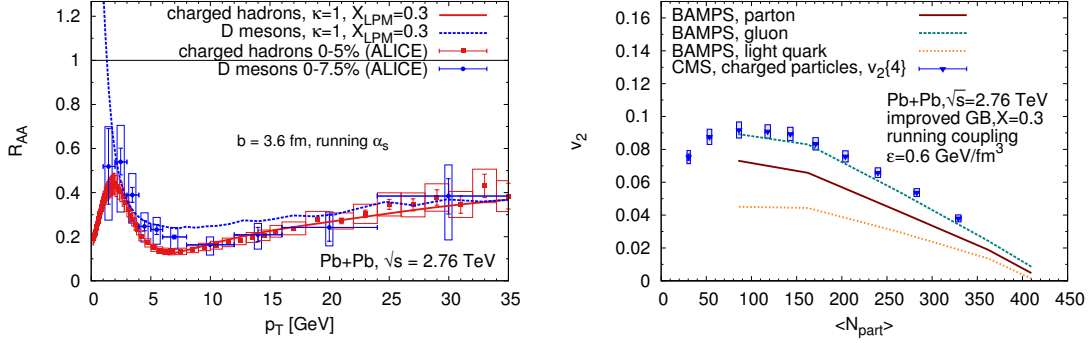
Figure 3: Left: Nuclear modification factor R_{AA} of charged hadrons and D mesons at LHC as published in Ref. [5] in comparison to data [16, 23]. Both binary and radiative processes with a LPM parameter set to $X_{LPM} = 0.3$ are considered. Right: Elliptic flow v_2 of gluons, light quarks, and both together (light partons) within $|\eta| < 0.8$ at LHC as a function of the number of participants N_{part} for a running coupling and LPM parameter $X = 0.3$ as published in Ref. [3]. As a comparison we show experimental data by CMS for charged hadrons within $|\eta| < 0.8$ [25].

a minimum at the phase transition. The value of η/s in the region around $T = 0.2\,\text{GeV}$ that is most important for the elliptic flow is approximately 0.2 for $n_f = 0$, which agrees very well with the shear viscosity extraction from dissipative hydrodynamic models employing a constant $\eta/s = 0.2$ together with initial fluctuations modeled by IP-Glasma [28]. Thus our calculation employing pQCD cross sections can give a microscopic explanation of the small shear viscosity to entropy density ratio extracted from hydrodynamics.

Besides the shear viscosity it is also possible to study other transport coefficients of the QGP medium, like e.g. the heat conductivity κ [39] or the electric conductivity σ_{el} [6]. The electric conductivity is related to the soft dilepton production rate and the diffusion of magnetic fields in the medium. Studies of the electric conductivity allows to compare the effective cross sections of medium constituents between several theories, including transport models [29, 40], lattice gauge theory [32, 33, 34, 35, 36, 37, 38] and Dyson-Schwinger calculations [41].

The longitudinal static electric conductivity σ_{el} relates the response of the electric diffusion current density $\vec{j}$ to an externally applied static electric field $\vec{E}$, $\vec{j} = \sigma_{\text{el}}\vec{E}$. Additionally, the electric conductivity can also be obtained by the Green-Kubo [42, 43] formula for the electric current density in x-direction $j_x(t)$,

$$\sigma_{\text{el}} = \beta V \int_0^\infty \langle j_x(0)j_x(t)\rangle\,\mathrm{d}t \quad \text{with} \quad j^x(t) = \frac{1}{VN_{\text{test}}} \sum_{k=1}^M q_k \sum_{i=1}^{N_k} \left.\frac{p_i^x}{p_i^0}\right|_t, \tag{3}$$

where V denotes the volume, $\beta = T^{-1}$ the inverse temperature, M the number of particle species and N_k the number of particles of species k. The electric current autocorrelation function $\langle j_x(0)j_x(t)\rangle$ can be obtained numerically, as it has been done in e.g. Ref. [27] for the shear stress tensor correlation function.

By employing BAMPS with the described pQCD cross sections, it is possible to extract
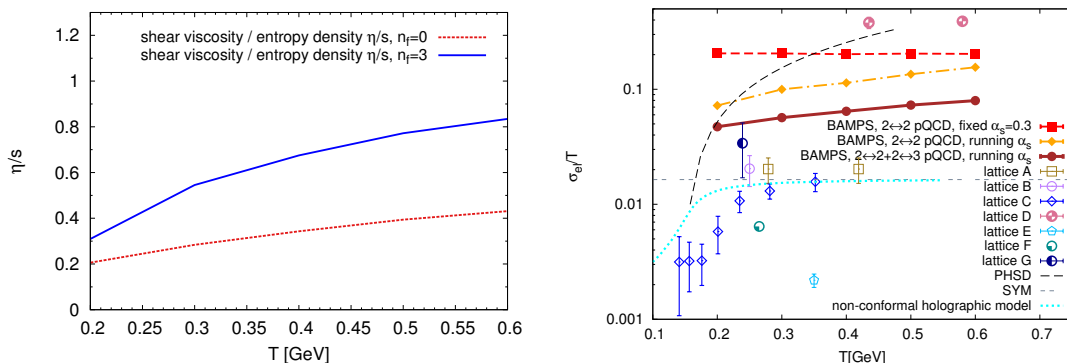
Figure 4: Left: Shear viscosity over entropy density η/s for running coupling and $X_{\mathrm{LPM}} = 0.3$ in a static medium of temperature T with number of quark flavors n_f as published in Ref. [3]. Right: Electric conductivity σ_{el} within BAMPS (filled symbols) as published in Ref. [6] compared to recent results from literature. The open symbols represent results from lattice QCD. PHSD: [29], SYM: [30], non-conformal holographic model: [31], lattice A: [32], lattice B: [33], lattice C: [34], lattice D: [35], lattice E: [36], lattice F: [37], lattice G: [38]. The electric charge is explicitly multiplied out, $e^2 = 4\pi/137$.

the electric conductivity of a plasma consisting of quarks and gluons in the massless limit using both approaches, via the response of the electric diffusion current density and the Green-Kubo relation. These studies have shown that both methods show identical results [6], what has been additionally justified by comparison with analytically formulas employing constant, isotropic cross sections. Figure 4 depicts the results for the electric conductivity using pQCD cross sections together with either a running coupling or a fixed coupling $\alpha_s = 0.3$. The electric conductivity reflects in a profound way the effect of inelastic pQCD scatterings and the running of the coupling α_s. The presented results from the BAMPS transport simulation lie between $0.04 \leq \sigma_{\mathrm{el}}/T \leq 0.08$ for temperatures 0.2 GeV $\leq T \leq 0.6$ GeV. As a remark, the quantitative comparison with lattice QCD data is difficult since the published results from lattice QCD for the electric conductivity vary widely between $0.001 \leq \sigma_{\mathrm{el}}/T \leq 0.1$.

6 Conclusions

By solving the relativistic Boltzmann equation for on-shell partons, the partonic transport approach BAMPS allows the full 3+1D microscopic simulation of the QGP created in ultra-relativistic heavy-ion collisions. Consequently, investigations of both the suppression of high p_t particles and the collectivity of the bulk medium within a common framework are possible within BAMPS. By employing an improved Gunion-Bertsch matrix element and a running coupling evaluated at the microscopic level, we are able to describe high p_t and heavy flavor observables at LHC. Furthermore, the same microscopic pQCD interactions lead to a sizable elliptic flow of the bulk medium within the partonic phase. Furthermore, we investigated medium properties of the QGP in terms of the shear viscosity to entropy density ratio η/s and the electric conductivity σ_{el} from a microscopic perspective.

FLORIAN SENZEL, MORITZ GREIF, JAN UPHOFF, CHRISTIAN WESP, ZHE XU, . . .

Acknowledgments

References

[1] Berndt Müller, Jurgen Schukraft, and Boleslaw Wyslouch. First Results from Pb+Pb collisions at the LHC. *Ann.Rev.Nucl.Part.Sci.*, 62:361–386, 2012.

[2] Florian Senzel, Oliver Fochler, Jan Uphoff, Zhe Xu, and Carsten Greiner. Influence of multiple in-medium scattering processes on the momentum imbalance of reconstructed di-jets. arXiv:1309.1657, 2013.

[3] Jan Uphoff, Oliver Fochler, Florian Senzel, Christian Wesp, Zhe Xu, et al. Elliptic flow and nuclear modification factor in ultra-relativistic heavy-ion collisions within a partonic transport model. arXiv:1401.1364, 2014.

[4] Jan Uphoff, Oliver Fochler, Zhe Xu, and Carsten Greiner. Open Heavy Flavor in Pb+Pb Collisions at $\sqrt{s} = 2.76$ TeV within a Transport Model. *Phys.Lett.*, B717:430–435, 2012.

[5] Jan Uphoff, Oliver Fochler, Zhe Xu, and Carsten Greiner. Elastic and radiative heavy quark interactions in ultra-relativistic heavy-ion collisions. arXiv:1408.2964, 2014.

[6] Moritz Greif, Ioannis Bouras, Zhe Xu, and Carsten Greiner. Electric Conductivity of the Quark-Gluon Plasma investigated using a pQCD based parton cascade. arXiv:1408.7049, 2014.

[7] Zhe Xu and Carsten Greiner. Thermalization of gluons in ultrarelativistic heavy ion collisions by including three-body interactions in a parton cascade. *Phys.Rev.*, C71:064901, 2005.

[8] Zhe Xu and Carsten Greiner. Transport rates and momentum isotropization of gluon matter in ultrarelativistic heavy-ion collisions. *Phys.Rev.*, C76:024911, 2007.

[9] J.F. Gunion and G. Bertsch. Hadronization by color bremsstrahlung. *Phys.Rev.*, D25:746, 1982.

[10] Oliver Fochler, Jan Uphoff, Zhe Xu, and Carsten Greiner. Radiative parton processes in perturbative QCD – an improved version of the Gunion and Bertsch cross section from comparisons to the exact result. *Phys.Rev.*, D88:014018, 2013.

[11] Torbjorn Sjostrand, Stephen Mrenna, and Peter Skands. PYTHIA 6.4 physics and manual. *JHEP*, 05:026, 2006.

[12] Jan Uphoff, Oliver Fochler, Zhe Xu, and Carsten Greiner. Heavy quark production at RHIC and LHC within a partonic transport model. *Phys.Rev.*, C82:044906, 2010.

[13] S. Albino, B.A. Kniehl, and G. Kramer. AKK Update: Improvements from New Theoretical Input and Experimental Data. *Nucl.Phys.*, B803:42–104, 2008.

[14] Georges Aad et al. Observation of a Centrality-Dependent Dijet Asymmetry in Lead-Lead Collisions at $\sqrt{s_{NN}} = 2.77$ TeV with the ATLAS Detector at the LHC. *Phys.Rev.Lett.*, 105:252303, 2010.

[15] Serguei Chatrchyan et al. Jet momentum dependence of jet quenching in PbPb collisions at $\sqrt{s_{NN}} = 2.76$ TeV. *Phys.Lett.*, B712:176–197, 2012.

[16] Betty Abelev et al. Centrality Dependence of Charged Particle Production at Large Transverse Momentum in Pb–Pb Collisions at $\sqrt{s_{NN}} = 2.76$ TeV. *Phys.Lett.*, B720:52–62, 2013.

[17] Jan Uphoff, Oliver Fochler, Zhe Xu, and Carsten Greiner. Heavy quarks at RHIC and LHC within a partonic transport model. *Nucl.Phys.*, A855:444–447, 2011.

[18] Jan Uphoff, Oliver Fochler, Zhe Xu, and Carsten Greiner. Elliptic flow and energy loss of heavy quarks in ultra-relativistic heavy ion collisions. *Phys.Rev.*, C84:024908, 2011.

[19] B. Abelev et al. D meson elliptic flow in non-central Pb-Pb collisions at $\sqrt{s_{NN}} = 2.76$TeV. *Phys.Rev.Lett.*, 111:102301, 2013.

[20] Shingo Sakai. Measurement of R_{AA} and ν_2 of electrons from heavy-flavour decays in Pb-Pb collisions at $\sqrt{s_{NN}} = 2.76$ TeV with ALICE. *Nucl.Phys.*, A904-905:661c–664c, 2013.

[21] Zaida Consesa del Valle. Heavy-flavor suppression and azimuthal anisotropy in Pb-Pb collisions at $\sqrt{(s_{NN})} = 2.76$ TeV with the ALICE detector. *Nucl.Phys.*, A904-905:178c–185c, 2013.

[22] Betty Abelev et al. Production of muons from heavy flavour decays at forward rapidity in pp and Pb-Pb collisions at $\sqrt{s_{NN}} = 2.76$ TeV. *Phys.Rev.Lett.*, 109:112301, 2012.

[23] Alessandro Grelli. *D* meson nuclear modification factors in Pb-Pb collisions at $\sqrt{s_{NN}} = 2.76$ TeV with the ALICE detector. *Nucl.Phys.*, A904-905:635c–638c, 2013.

[24] Serguei Chatrchyan et al. Suppression of non-prompt J/psi, prompt J/psi, and Y(1S) in PbPb collisions at $\sqrt{s_{NN}} = 2.76$ TeV. *JHEP*, 1205:063, 2012.

[25] Serguei Chatrchyan et al. Measurement of the elliptic anisotropy of charged particles produced in PbPb collisions at nucleon-nucleon center-of-mass energy = 2.76 TeV. *Phys.Rev.*, C87:014902, 2013.

[26] Zhe Xu and Carsten Greiner. Elliptic flow of gluon matter in ultrarelativistic heavy- ion collisions. *Phys.Rev.*, C79:014904, 2009.

[27] C. Wesp, A. El, F. Reining, Z. Xu, I. Bouras, et al. Calculation of shear viscosity using Green-Kubo relations within a parton cascade. *Phys.Rev.*, C84:054911, 2011.

[28] Charles Gale, Sangyong Jeon, Bjorn Schenke, Prithwish Tribedy, and Raju Venugopalan. Event-by-event anisotropic flow in heavy-ion collisions from combined Yang-Mills and viscous fluid dynamics. *Phys.Rev.Lett.*, 110:012302, 2013.

[29] W. Cassing, O. Linnyk, T. Steinert, and V. Ozvenchuk. Electrical Conductivity of Hot QCD Matter. *Physical Review Letters*, 110(18):182301, May 2013.

[30] Simon C Huot, Pavel Kovtun, Guy D Moore, Andrei Starinets, and Laurence G. Yaffe. Photon and dilepton production in supersymmetric Yang-Mills plasma. *Journal of High Energy Physics*, 2006(12):015–015, December 2006.

[31] S. I. Finazzo and Jorge Noronha. Holographic calculation of the electric conductivity of the strongly coupled quark-gluon plasma near the deconfinement transition. *Physical Review D*, 89(10):106008, May 2014.

[32] Gert Aarts, Chris Allton, Justin Foley, Simon Hands, and Seyong Kim. Spectral functions at small energies and the electrical conductivity in hot quenched lattice QCD. *Physical Review Letters*, 99(2):022002, 2007.

[33] Bastian B. Brandt, Anthony Francis, Harvey B. Meyer, and Hartmut Wittig. Thermal correlators in the ρ channel of two-flavor QCD. *Journal of High Energy Physics*, 2013(3):100, March 2013.

[34] Alessandro Amato, Gert Aarts, Chris Allton, Pietro Giudice, Simon Hands, and Jon-Ivar Skullerud. Electrical Conductivity of the Quark-Gluon Plasma Across the Deconfinement Transition. *Physical Review Letters*, 111(17):172001, October 2013.

[35] Sourendu Gupta. The electrical conductivity and soft photon emissivity of the QCD plasma. *Physics Letters B*, 597(1):57–62, September 2004.

[36] P. V. Buividovich, M. N. Chernodub, D. E. Kharzeev, T. Kalaydzhyan, E. V. Luschevskaya, and M. I. Polikarpov. Magnetic-Field-Induced Insulator-Conductor Transition in SU(2) Quenched Lattice Gauge Theory. *Physical Review Letters*, 105(13):132001, September 2010.

[37] Y Burnier and M Laine. Towards flavour-diffusion coefficient and electrical conductivity without ultraviolet contamination. *The European Physical Journal C*, 72(2):1–8, 2012.

[38] H.-T. Ding, A. Francis, O. Kaczmarek, F. Karsch, E. Laermann, and W. Soeldner. Thermal dilepton rate and electrical conductivity: An analysis of vector current correlation functions in quenched lattice QCD. *Physical Review D*, 83(3):034504, February 2011.

[39] M. Greif, F. Reining, I. Bouras, G.S. Denicol, Z. Xu, and C. Greiner. Heat conductivity in relativistic systems investigated using a partonic cascade. *Physical Review E*, 87(3):033019, March 2013.

[40] T. Steinert and W. Cassing. Electric and magnetic response of hot QCD matter. *Physical Review C*, 89(3):035203, March 2014.

[41] Si-xue Qin. A Divergence-Free Method to Extract Observables from Meson Correlation Functions. arXiv:1307.4587, 2013.

[42] Melville S. Green. Markoff Random Processes and the Statistical Mechanics of Time-Dependent Phenomena. II. Irreversible Processes in Fluids. *The Journal of Chemical Physics*, 22(3):1281, 1952.

[43] Ryogo Kubo. Statistical-Mechanical Theory of Irreversible Processes. I. General Theory and Simple Applications to Magnetic and Conduction Problems. *Journal of the Physical Society of Japan*, 12(6):570–586, June 1957.